

Multi-objective optimization for the geometry of trapezoidal corrugated morphing skins

Iman Dayyani¹ · Michael I. Friswell²

Received: 3 July 2015 / Revised: 26 April 2016 / Accepted: 27 April 2016 / Published online: 11 May 2016
© The Author(s) 2016. This article is published with open access at Springerlink.com

Abstract Morphing concepts have great importance for the design of future aircraft as they provide the opportunity for the aircraft to adapt their shape in flight so as to always match the optimal configuration. This enables the aircraft to have a better performance, such as reducing fuel consumption, toxic emissions and noise pollution or increasing the maneuverability of the aircraft. However the requirements of morphing aircraft are conflicting from the structural perspective. For instance the design of a morphing skin is a key issue since it must be stiff to withstand the aerodynamic loads, but flexible to enable the large shape changes. Corrugated sheets have remarkable anisotropic characteristics. As a candidate skin for a morphing wing, they are stiff to withstand the aerodynamic loads and flexible to enable the morphing deformations. This work presents novel insights into the multi-objective optimization of a trapezoidal corrugated core with elastomer coating. The geometric parameters of the coated composite corrugated panels are optimized to minimize the in-plane stiffness and the weight of the skin and to maximize the flexural out-of-plane stiffness of the skin. These objective functions were calculated by use of an equivalent finite element code. The gradient-based aggregate method is selected to solve the optimization problem and is validated by comparing to the GA multi-objective optimization technique. The trend of the optimized objectives and parameters are discussed in detail; for example

the optimum corrugation often has the maximum corrugation height. The obtained results provide important insights into the design of morphing corrugated skins.

Keywords Multi objective optimization · Corrugated · Morphing

1 Introduction

1.1 About morphing aircraft

Improving the performance of an aircraft is important for a variety of reasons, such as: reducing the energy consumption, decreasing the toxic emissions and noise pollution or increasing the maneuverability of the aircraft (Barbarino et al. 2011; Chekkal et al. 2014). The only way of achieving these objectives is through better engines, more aerodynamically efficient wings, and lighter structures. However, the problem with the design of current aircraft wings is that they cannot be optimized for every single point of the flight envelope, for example take off, cruise and landing. In other words the wings of an aircraft are a compromise that limits the flight to a range of conditions where the performance of the aircraft at each condition is sub-optimal. Hence, a new generation of aircraft known as morphing aircraft are needed for further improvement of the aircraft performance without unacceptable penalties in terms of cost, complexity and weight. Compliant structures and mechanisms with highly anisotropic mechanical behavior enable these aircraft to adapt their shape in flight so as to always match the optimal configuration. In contrast to conventional aircraft design, the new morphing technology provides higher efficiency in terms of lightness, size of volume, energy consumption and mission diversity.

✉ Iman Dayyani
I.Dayyani@Cranfield.ac.uk

¹ Centre for Structures, Assembly and Intelligent Automation, School of Aerospace, Transport and Manufacturing, Cranfield University, Cranfield MK43 0AL, UK

² College of Engineering, Swansea University Bay Campus, Swansea SA1 8EN, UK

1.2 Corrugation and anisotropic behavior

The requirements for morphing aircraft are conflicting. For instance, the skin is a critical component of the morphing wing and must be stiff to withstand the aerodynamic loads, but also must be flexible to enable the shape changes. Corrugated sheets have exceedingly anisotropic behaviour; they are stiff along the corrugation direction, but flexible in the transverse direction. For this reason, coated composite corrugated panels have been proposed as a candidate morphing skin (Dayyani et al. 2015a). Corrugated panels have other remarkable characteristics, such as a high ratio of strength to density, good energy absorption and easy fabrication. Hence many papers have been published in the literature investigating the mechanical behavior of corrugated sheets for general applications, such as the effect of different shapes of the corrugation on the bending stiffness of the panel (Luo et al. 1992), their geometric and material nonlinearities with different loading configurations through finite element analysis (Gilchrist et al. 1999), the equivalent properties of the panels by homogenized-based analytical models (Bartolozzi et al. 2014) and the dynamic response of corrugated sandwich panels in free vibration analysis (Peng et al. 2014) or under air blast loadings (Li et al. 2014; Zhang et al. 2014).

1.3 Morphing skin and corrugation

The development of smart materials and adaptive structures motivated designers to consider corrugated sheets in morphing skin applications. Researchers have studied the detailed nonlinear mechanical behaviour of composite corrugated sheets through experimental and numerical models. These models were used as a base for further homogenization studies that retained the dependence on the geometric parameters of the corrugated panels (Dayyani et al. 2014; Mohammadi et al. 2015; Shaw et al. 2015). The open question regarding the applicability of the papers in the literature to system level optimization in morphing aircraft was considered in (Dayyani et al. 2015b). In this paper, Dayyani et al. proposed and justified the design of corrugated skins on top of a morphing internal structure known as FishBAC (Fish Bone Active Camber). The FishBAC internal structure consists of a thin chord wise bending beam spine with stringers branching off to connect the spine to the skin surface. They highlighted the interaction of corrugated skin with both the internal structure and the air flow in the real application. They discussed that the out-of-plane deformation of the skin is the most influential factor on the aerodynamic performance of the wing and can occur due to buckling of the skin while actuating the internal structure and due to the distribution of aerodynamic loading.

In this paper a general procedure for the multi objective optimization of a corrugated morphing skin is presented.

The multi objective optimization is performed in terms of three objective functions: the mass of the skin, the tensile in-plane stiffness and the flexural out-of-plane stiffness. A finite element code for thin beam elements is written in MATLAB to calculate the equivalent tensile and flexural stiffness of the corrugated morphing skin. The gradient-based aggregate method is used to perform the multi-objective optimization and the corresponding results are validated by comparing to those data obtained by the GA multi-objective optimization technique. The strengths and limitations of each method are then highlighted through the comparison. The trend of the optimized objectives and parameters are discussed in detail which provides a good insight into the design of corrugated morphing skins. The obtained results are very encouraging and the described procedure can be applied to more complex analyses such as uncertainty analysis and the robust optimization problem.

2 Problem statement

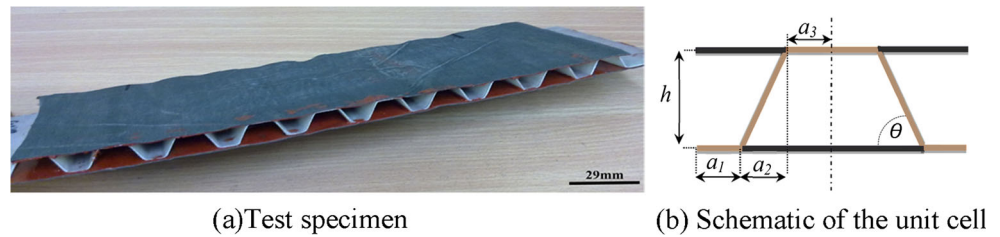
Among different typical shapes of corrugation, the trapezoidal profile has better performance with regard to the morphing application. The coated corrugated core with trapezoidal corrugation profile has higher out-of-plane stiffness and lower in-plane stiffness than other shapes. The higher out-of-plane stiffness of the skin results in a smoother surface of the wing during flight, while lower in-plane stiffness results in smaller energy requirements for morphing actuation. For this reason the trapezoidal corrugation shape is selected for the optimization of corrugated skin.

2.1 Equivalent properties of the coated corrugated core

The equivalent tensile and flexural stiffnesses and the mass of a coated trapezoidal corrugated core were calculated using a finite element code which considers 4 unit cells of corrugation. The parameters a_1 , a_2 , a_3 and h defining the geometry of a trapezoidal corrugated unit cell (as shown in Fig. 1b), and t_c and t_e representing the thickness of the corrugated core and elastomeric coating, were the inputs of this FE code in MATLAB. The material properties were defined by means of ρ_c and ρ_e representing the density of the composite core and the elastomeric coating, and E_c and E_e representing the Young's modulus of the composite core and the elastomeric coating. Since the ratio of the elastomer Young's modulus to the glass fiber Young's modulus is very small, a reasonable assumption is to neglect the elastomer coating in the areas overlapped with the composite corrugated core (Dayyani et al. 2013).

Two translational degrees of freedom and one rotational degree of freedom in the global coordinate system were considered at each node. The coated corrugated structure was

Fig. 1 Trapezoidal corrugated core with elastomeric coating (Dayyani et al. 2013)



discretized by 26 beam elements. The difference between the equivalent properties of a long corrugated panel and a corrugated panel with 4 unit cells was examined in ABAQUS and was smaller than 1 %. The finite element code calculating the equivalent properties was a function called in the optimization solver.

2.2 Multi objective optimization

Figure 2 illustrates the geometry of the proposed design of corrugated skin on top of a morphing internal structure, namely the FishBAC (Dayyani et al. 2015b). The length of the morphing section in this design, i.e. l_{morph} , between the rigid leading edge and rigid trailing edge, was 160 mm, which is equivalent to 52 % of the chord length. The number of FishBAC stringers, n_s , was allowed to vary between 3 and 15. Based on the distance between two adjacent stringers (i.e. $d_s = l_{morph} / (n_s + 1)$) and manufacturing constraints the number of corrugation unit cells, N_u , was allowed to vary from 1 to $N_{u-final}$, which is calculated by rounding down the ratio d_s / L_{uc-a} . The parameter L_{uc-a} refers to the minimum allowable length of a corrugation unit cell which was set to 5 mm due to manufacturing limits. In other words, n_s and N_u can be considered as an implicit constraints on the length of the corrugation unit cell in the optimization procedure:

$$L_{unitcell} = \frac{l_{morphing}}{(N_{stringers} + 1)N_{unitcell}} \tag{1}$$

(1) is derived by combining $L_{unitcell} = \frac{d_{stringers}}{N_{unitcell}}$ and $d_{stringers} = \frac{l_{morphing}}{(N_{stringers} + 1)}$. Table 1 presents the range of the corrugation unit cell lengths corresponding to different possible

configurations of FishBAC stringers and the corrugated skin.

Table 1 show that increasing the number of stringers reduces the range of the number of unit cells due to the minimum allowable length restriction. This results in the non-uniform increasing increments of corrugation unit cell lengths. The height of the rigid part at the end of trailing edge, which is shown as l_{rt} in Fig. 2, was used as a criterion of the upper bound for the height of the corrugated unit cell. The value for this parameter was estimated as 5.21 mm in the FishBAC geometry.

The materials for the composite core and the elastomer coating of the corrugated skin are selected from the literature. The density of composite corrugated core and elastomer coating were 1799 and 878 kg/m³, while their equivalent isotropic Young’s moduli were 34,473 and 10 MPa respectively. It should be mentioned here that these material properties correspond to fiber glass composite and synthetic rubber, namely polyurethane (PU). Although, a full optimization of both geometry and material properties of the corrugated morphing skin may be necessary, this article is focused on the geometrical parameters of the skin to highlight their effects on the mechanical behavior of the structure in a more sensible manner .

Table 2 shows the geometrical parameters of a coated corrugated core unit cell (as shown in Fig. 1b) and their corresponding upper and lower bounds.

Selecting the upper and lower bounds for the thickness of both the corrugated core and the elastomeric coatings was based on practical considerations. The properties of the corrugated skin arise from localized bending within the corrugations; if the ratio of the thickness of the corrugated core to the length of a unit cell is too high, then the mechanism of the deformation changes, resulting in a panel that is too stiff, especially when the size of the corrugation is very small. The lower bounds are set by the availability of suitable material

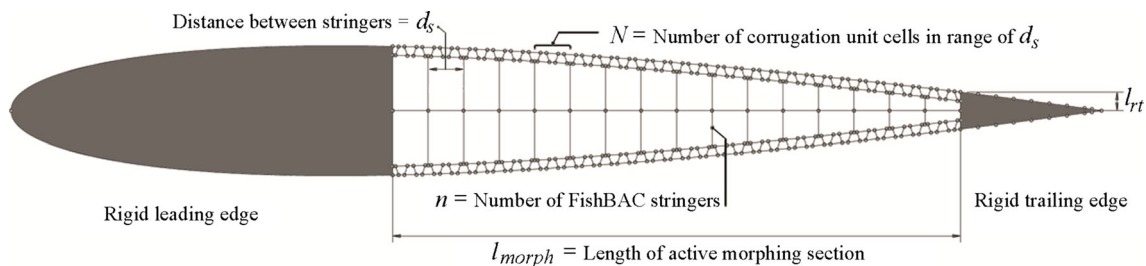


Fig. 2 Corrugated morphing skin on top of a FishBAC internal structure (Dayyani et al. 2015b)

Table 1 A range of the corrugation unit cell lengths corresponding to different configurations of FishBAC stringers and the corrugated skin

Length of Unit Cells(mm)	5	5.33	5.71	5.93	6.15	6.40	6.67	7.27	7.62	8	8.89	10	
	10.67	11.43	12.31	13.33	14.55	16	17.78	20	22.86	26.67	32	40	
$n_{stringers}$	3	4	5	6	7	8	9	10	11	12	13	14	15
$N_{unitcells}$	[1-8]	[1-6]	[1-5]	[1-4]	[1-4]	[1-3]	[1-3]	[1-2]	[1-2]	[1-2]	[1-2]	[1-2]	[1-2]

and its robustness and handling properties. The upper bound and lower bound for a_1, a_2, a_3 were selected to be consistent with the geometry of a trapezoidal shape. Considering the application of the corrugated panel for a morphing skin, the height of the corrugated unit cell is dependent on the external parameter l_{rt} which is the maximum size that the height of the panel can be. Based on Fig. 1b the equation $a_1 + a_2 + a_3 = (L_{UC}/2)$ was considered as the only explicit constraint of the optimization problem, where L_{UC} represents the length of a unit cell and is implicitly constrained by the number of FishBAC stringers and the number of corrugation unit cells. The following three objectives are minimized: the equivalent tensile stiffness EA_{eq} , the inverse of the equivalent flexural stiffness $\frac{1}{EI_{eq}}$ and the mass of the skin. In order to ensure the best performance of the optimization scheme all the parameters were normalized between -1 and +1. The normalized objective functions were also calculated based on their value at the average parameter values.

2.3 Selection of the multi-objective optimization method

In general two different types of techniques are used to solve multi objective optimization problems. These two types are known as classical methods and evolutionary methods. The classical methods, which are mainly non-Pareto based techniques, consist of converting the multi objective problem into a single objective problem. This is possible by either aggregating the objective functions or optimizing one objective and treating the other as constraints. This new single objective function will then be optimized for different configurations of weights of the objective functions. The classic aggregate method is easy to implement especially for a few objectives

and is efficient for some multi-objective optimization problems with convex Pareto fronts (Izui et al. 2015). On the other hand the evolutionary methods mainly use non dominated ranking and selection, to move the population towards the Pareto front. These methods require a ranking procedure and a technique to maintain the diversity in the population so as to avoid converging to a single solution, because of the stochastic noise involved in this process. These evolutionary approaches are less susceptible to the shape or continuity of the Pareto front. However, in many cases the Pareto curves cannot be computed efficiently, even if it is theoretically possible to find of all these points exactly, which is why approximation methods for these techniques are frequently used. In this section the aggregate method from the classic methods and the Genetic Algorithm (GA) from the evolutionary techniques are used to solve the multi objective optimization problem for a unit cell length of 10 mm corresponding to specific cases 3.4, 7.2 and 15.1. It should be mentioned here that in this nomenclature the numbers before and after the “.” refer to the number of FishBAC stringers and corrugation unit cells, respectively. For example case 15.1 refers to $n_{stringer}=15$ and $N_{unitcell}=1$. The results obtained from both methods are compared and the multi-objective optimization technique used in this paper is selected. It should be noted that the GA approach may be more beneficial for the system level optimization, which includes integer parameters for the number of stringers and corrugation unit cells.

2.3.1 Gradient based aggregate method

In this section the multi-objective problem is solved by combining three objectives into a single-objective scalar function.

Table 2 The parameters of the optimization problem and their upper and lower bounds

Parameters	t_c	t_e	a_1	a_2	a_3	h
Delineation	Thickness of		Corrugation unit cell geometry (Fig. 1b)			
	Corrugated core	Elastomer coating				
Lower bound	$L_{UC}/60$ (mm)	$L_{UC}/60$ (mm)	$L_{UC}/12$ (mm)	$L_{UC}/12$ (mm)	$L_{UC}/12$ (mm)	$l_{rt}/2$ (mm)
Upper bound	$L_{UC}/30$ (mm)	$2L_{UC}/30$ (mm)	$L_{UC}/3$ (mm)	$L_{UC}/3$ (mm)	$L_{UC}/3$ (mm)	$9l_{rt}/10$ (mm)

This approach is also known as the “weighted-sum” or “scalarization” method. In more detail, the aggregate method minimizes a positively weighted convex sum of the objectives, i.e. $\min \sum_{j=1}^3 w_j f_j(\zeta)$. This new single objective optimization problem is then solved using the “fmincon” command which is a gradient based method in MATLAB. This method is appropriate for problems where the objective and constraint functions are both continuous and have continuous first derivatives; this does not cause any restriction on the use of this method for this optimization problem as continuous analytical solutions have been proposed for the mechanical behavior of these structures. Weighting coefficients in this equation are positive and represent the relative importance of the objective functions $f_j(\zeta)$ and ζ is the vector of the input parameters in the optimization problem. It is assumed that the sum of the weighting coefficients is equal to one, i.e. $\sum_{j=1}^3 w_j = 1$. This technique is ideal for cases where preferential information about the objectives is known in advance. However, it is possible to achieve the non-dominated front by considering a broader interval of the aggregation parameters. Since the solutions of this optimization problem can vary significantly as the weighting coefficients change, and because very little is usually known about choosing these coefficients, it is necessary to solve the same problem for many different values of these weights. Adaptive weighting algorithms may be used to generate a good representation of the Pareto curve, although further evaluations of a bi-level optimization problem are needed in this regard (Zhang and Gao 2006). However, the weights were considered to vary from 0.01 to 0.99 in increments of 0.01. While the aggregate method is simple to implement, it has some limitations and drawbacks. For instance, obtaining points on non-convex portions of the Pareto optimal set is impossible and varying the weights consistently and continuously may not necessarily result in an even distribution of Pareto optimal points (Das and Dennis 1997). The results obtained by this method are presented in Section 2.3.3 for the unit cell length of 10 mm corresponding to the specific cases 3.4, 7.2 and 15.1.

2.3.2 Pareto based GA method

Normally, the multi-objective optimization problems are conflicting in nature and hence there does not exist a single solution that simultaneously optimizes all objectives. A change in the optimization parameters of an individual point which makes at least the value of one objective function better without making any others worse, is called a Pareto improvement. A set of individuals are then defined as “Pareto optimal” when no further Pareto improvements are possible. There are many different techniques in the literature (Hochman and Rodgers

1969; Deb 2001; Marler and Arora 2004) to select the Pareto optimal set, which are beyond the scope of this paper. In this section the multi-objective problem is solved using the Pareto based GA technique in MATLAB. More details of the fundamentals of genetic algorithms can be found in (Munk et al. 2015; Goldberg and Holland 1988).

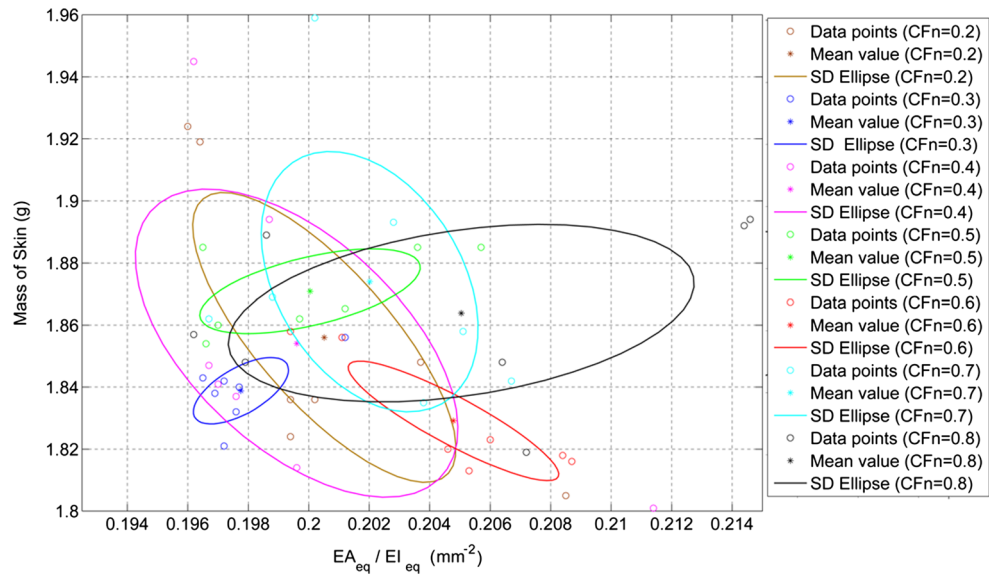
In this section the multi objective optimization problem is solved by use of the “gaoptimset” command in MATLAB. All settings were considered as default except two: the population size and the crossover fraction. First with the fixed population size of 200 the effect of crossover fraction was investigated. Neglecting the elite children in each generation, the crossover fraction coefficient specifies the ratio of the crossover children to mutation children. For instance a crossover fraction of 1 means that all children other than elite individuals are crossover children, while a crossover fraction of 0 means that all children are mutation children. In fact neither of these extremes is an effective strategy to optimize a function and the best value for crossover fraction is dependant to the nature of the optimization problem. To select the best crossover fraction in this problem, a set of different crossover coefficients of [0.2, 0.3, ..., 0.8] was considered. With each cross over coefficient, seven optimization runs were performed and the corresponding best compromise point was selected. Figure 3 shows the means and standard deviations of the best compromise point in all of these optimization runs for each value of the crossover fraction.

It is evident in Fig. 3 that for this multi objective problem, setting the crossover fraction to 0.3 yields the best result since it has the minimum deviation and minimum mean value for each objective functions. Due to the stochastic behaviour of the genetic algorithm this procedure must be done prior to the proper use of this method. In Fig. 3 the two objectives of EA_{eq} and $\frac{1}{EI_{eq}}$ are combined into $\frac{EA_{eq}}{EI_{eq}}$, to produce a better illustration as a 2D standard deviation rather than a 3D standard deviation. Another parameter which increases the efficiency of the Pareto front in GA is the size of the population. Population sizes of [50, 100, 200, 400] were tried in the optimization and finally a population size of 200 was selected because of time efficiency and better fitness values. The results obtained by the GA method are presented in Section 2.3.3. for a unit cell length of 10 mm corresponding to specific cases 3.4, 7.2 and 15.1.

2.3.3 Comparison of the GA and aggregate methods

The gradient based aggregate method differs from the GA in two main ways. The aggregate method generates a single point at each iteration and the next point is selected in the sequence by a deterministic computation. At the end the sequence of points approaches the optimal solution. On the other hand the genetic algorithm generates a population of

Fig. 3 Standard deviation analysis of the crossover fraction effect in the GA, and selection of CFn=0.3 in the optimization problem

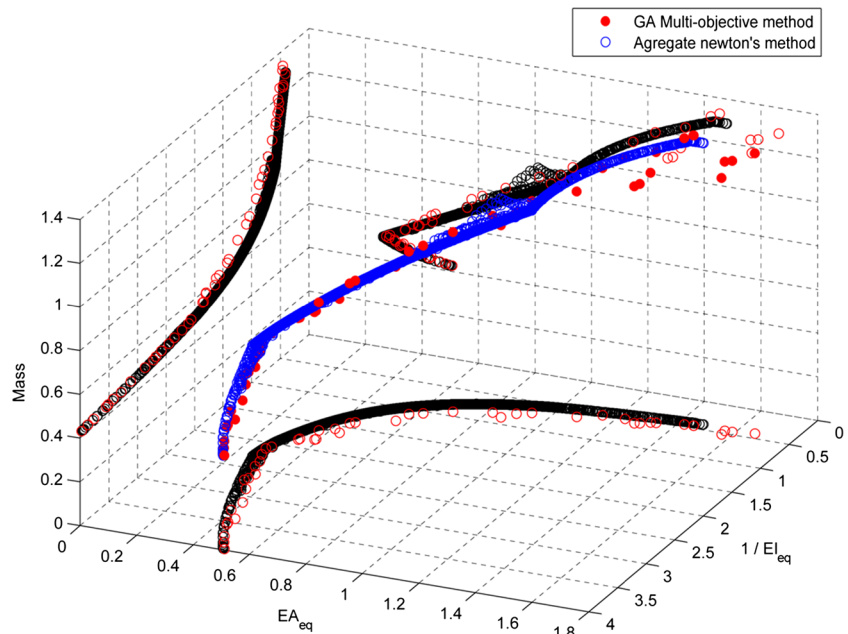


individuals at each iteration and the next population is selected by stochastic computation. Finally the points with higher ranking in the population approach the Pareto optimal.

Figure 4 shows the normalized optimum Pareto surface and its projection on three planes for the unit cell length of 10 mm corresponding to the specific cases 3.4, 7.2 and 15.1. In this figure the red and black points correspond to the GA multi objective and the gradient aggregate methods respectively. Figure 4 shows a non-convex curvature of the Pareto front of the multi objective optimization problem and there is a difference in the smoothness of the Pareto front obtained from these two methods. As discussed earlier one of the main

drawbacks of the aggregate method is the inability to obtain points on non-convex portions of the Pareto optimal set. Hence before using the aggregate method there must be some information which verifies the non-convex curvature of the Pareto front. The verification here is obtained by observing the good correlation of results obtained by the aggregate method with those on the GA Pareto front. In addition Fig. 4 shows that the weight distribution in the aggregate problem has resulted in an even distribution of Pareto optimal points. Moreover the Pareto curve is less smooth for the genetic algorithm, compared to the gradient based aggregate method, which is due to the randomness and stochastic nature of the

Fig. 4 Comparison of the GA and the gradient based aggregate methods, for the unit cell length of 10 mm corresponding to specific cases 3.4, 7.2 and 15.1



genetic algorithm. Considering all these points, the gradient based aggregate method is selected to solve the multi-objective optimization problem described in Section 2.2.

3 Discussion

Selecting the proper method to solve the multi-objective optimization problem, the results were obtained for different numbers of FishBAC stringers and corrugation unit cells as presented in Table 1. Figures 5a and 6a show the normalized Pareto surface and its projection on three planes for the unit cell length of 17.78 mm corresponding to specific case 8.1 and the unit cell length of 5.33 mm corresponding to specific cases [4.6, 5.5, 9.3, 14.2]. The Pareto fronts for the other cases are similar to one of these two patterns. The best compromise point of these two configurations is also highlighted as red in Figs. 5a and 6a. The best compromise point was selected by first identifying the ideal reference point as the coordinates of minimum normalized objective values, i.e.:

$$P_{ref} = \left(\left(\frac{1}{EI_{eq}} \right)_{\min}, (EA_{eq})_{\min}, (Mass_{skin})_{\min} \right) \quad (2)$$

Then the point which had the minimum distance from the ideal reference point, in the normalized objective function space, was selected as the best compromise point. Table 3 presents the corresponding weights of the optimization technique, the real values of the objectives and the optimized parameters corresponding to the best compromise point for the unit cell lengths of 17.78 mm and 5.33 mm. The range of the weights shows that all of the three objectives are involved efficiently in the process of optimization for the best

compromise point. Another point which must be noted in Table 3 is the range of differences in the value of the optimized parameters and objectives in these two cases, which is due to contracting the size of the corrugation in contrast to increasing the number of stringers. The comparison of the best compromise point of these two cases implies that more desirable objective values will be attained by reducing the size of the corrugation.

Figures 5b and 6b show the effect of weight distribution on the Pareto surfaces for the unit cell lengths of 17.78 and 5.33 mm. Generally, the relative value of the weights reflects the relative importance of the objectives. The dominance of each objective function is highlighted when its corresponding weight is in range of [0.7–1]. In these Pareto surfaces, the relatively horizontal plane highlighted as magenta is obtained when the weight w_3 corresponding to the third objective, i.e. the mass of skin, is dominant. In other words this plane has mainly minimized the mass of the skin but not the two other objectives: $\frac{1}{EI_{eq}}$ and EA_{eq} . The plane highlighted as green is obtained when the w_1 , corresponding to the first objective i.e. $\frac{1}{EI_{eq}}$, is dominant since the two other objectives are not minimized significantly. Likewise the region highlighted as orange is obtained when the weight w_2 corresponding to the second objective is dominant.

4 Trends of parameters and objective functions

In order to investigate the trend of the optimized parameters and objectives at the best compromise points for all of the configurations of the FishBAC stringers and corrugation unit cells are collected and studied in this section. Figure 7 shows the trend of first optimized objective function $\frac{1}{EI_{eq}}$ for different

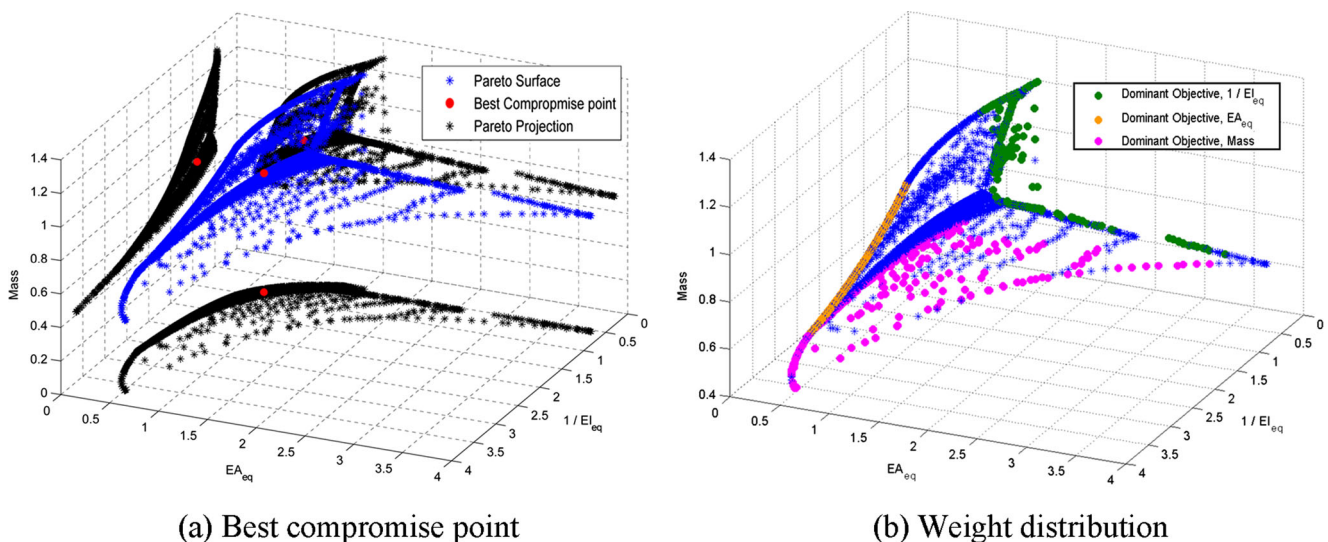


Fig. 5 Pareto surface for the unit cell length of 17.78 mm (case 8.1)

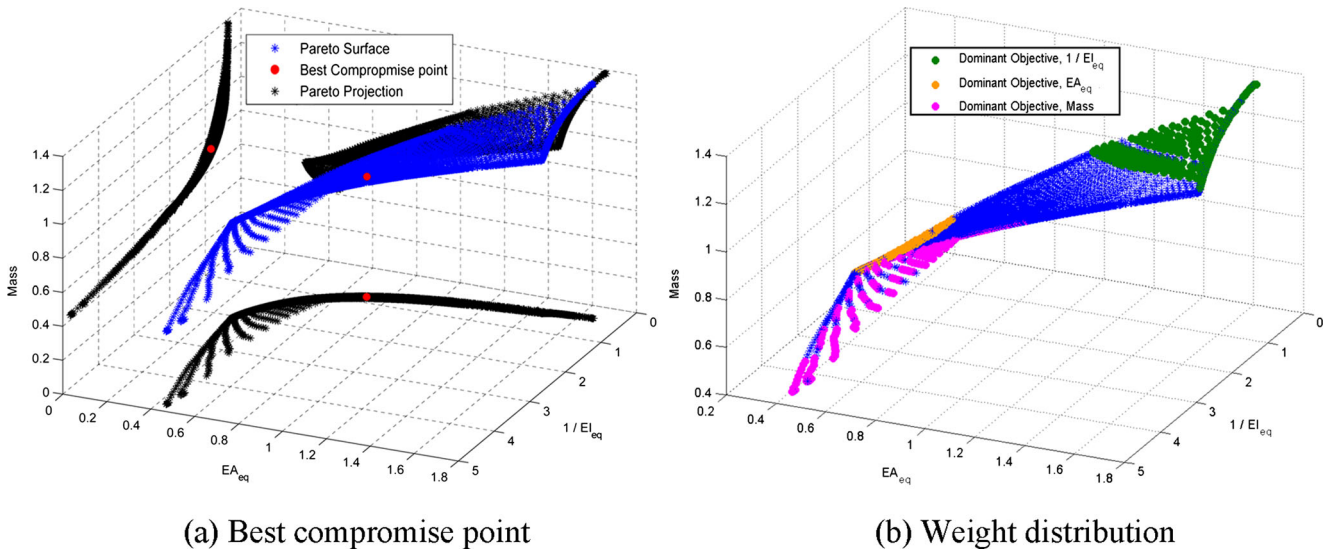


Fig. 6 Pareto surface for the unit cell length of 5.33 mm (cases [4.6, 5.5, 9.3, 14.2])

length of unit cells. Figure 7 shows that the out of plane compliance of the corrugated core with elastomeric coating decreases as the length of the corrugation unit cell increases. For a corrugated panel with a fixed length, as the length of the corrugation unit cells decreases the number of unit cells and consequently the number of corrugations increases. Thus the number of corners of a corrugated unit cell increases in the whole panel, as the corrugation unit cell gets smaller. These corners or corrugation lines which act like joints with torsional stiffness have the main role in the mechanism of deformation of corrugated structures. Hence the increase in the number of corrugation corners leads to more out of plane compliance of the panel. The minimum value for the out of plane compliance, which is obtained at $L_{uc} = 40\text{mm}$, is equal to $1.15 \times 10^{-5}(\text{N}.\text{mm})^{-2}$ as reported in the zoomed region provided in Fig. 7.

Figure 8 shows the trend of the second optimized objective function EA_{eq} for different lengths of unit cell. The in plane stiffness of the corrugated core with elastomeric coating

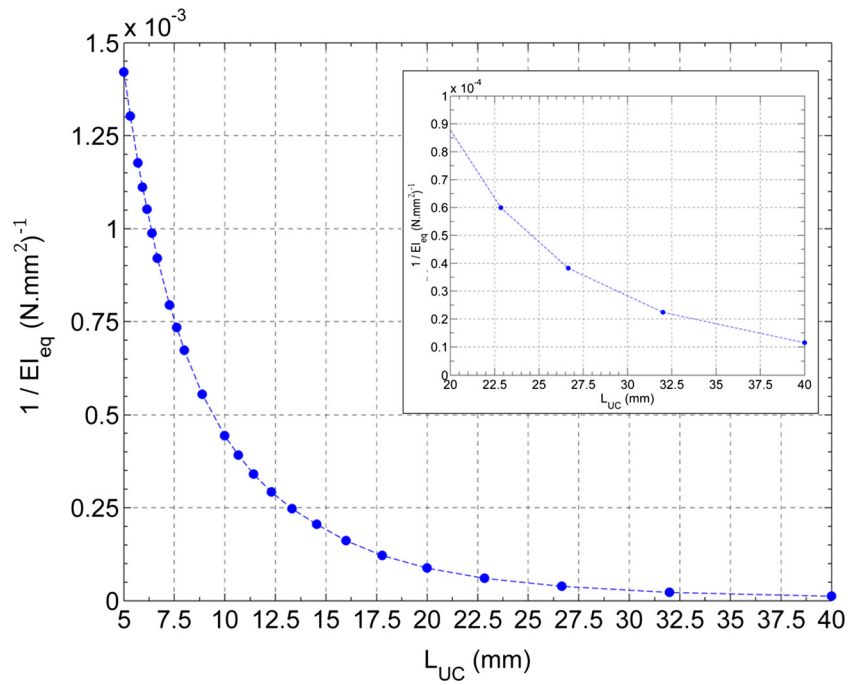
decreases as the length of the corrugation unit cell reduces. The minimum value for the in plane stiffness which is obtained at $L_{uc} = 5\text{mm}$ is equal to 139.5N as reported in the zoomed region provided in Fig. 8. With the same analogy the observed trend can be explained. As the corrugation unit cell gets smaller the number of corrugation lines increase in the whole panel and leads to more in-plane flexibility.

Comparing Figs. 7 and 8 suggests that the in plane and out of plane stiffness of the corrugated panel are correlated. In other words minimizing the in plane stiffness is conflicting with maximizing the out of plane stiffness. Figure 9 illustrates the linear behavior between the optimized in-plane stiffness and out of plane stiffness. This plot justifies the Fig. 3 in which two objective functions $\frac{1}{EI_{eq}}$ and EA_{eq} were combined into a single objective function $\frac{EA_{eq}}{EI_{eq}}$. The slope of the plot is about $0.21 (\text{mm})^{-2}$, which is in the range of values illustrated in Fig. 3 which were obtained by the GA multi objective optimization. The interesting point here is that although the trend

Table 3 Optimized properties of the best compromise points for the unit cell length of 17.78 mm (case 8.1) and the unit cell length of 5.33 mm (cases [4.6, 5.5, 9.3, 14.2])

Configuration of FishBAC stringers and corrugation unit cells	Weights			Real values of objectives			Optimized parameters					
	w_1	w_2	w_3	$\frac{1}{EI_{eq}}$ ($\text{N}.\text{mm}^2$) ⁻¹	EA_{eq} (N)	Mass of skin (g)	t_c (mm)	t_e (mm)	a_1 (mm)	a_2 (mm)	a_3 (mm)	h (mm)
$L_{UC} = 17.78$ (mm)	0.35	0.33	0.32	1.2×10^{-4}	1945	6.30	0.51	0.30	3.72	1.49	3.68	4.69
$L_{UC} = 5.33$ (mm)	0.40	0.36	0.24	1.3×10^{-4}	152.5	2.49	0.09	0.19	0.90	0.91	0.86	4.69

Fig. 7 The trend of optimized objective function $\frac{1}{EI_{eq}}$ for different lengths of unit cell



of both objectives in Figs. 7 and 8 are smooth the trend for the combination of them is non-smooth about EI_{eq} equivalent to $5000(N \cdot mm)^2$. The small jump in Fig. 9 may be explained by considering the domain of changes of parameters that gets smaller as the length of corrugation unit cells decrease as shown in Table 2. In other words the bounds for the points in Fig. 9 with $EI_{eq} \leq 5000$ make the domain of parameters tighter in contrast to the rest of points and hence they have different linear trend.

Figure 10 shows the trend of the third optimized objective function “mass” for different lengths of unit cell. The trend implies that, for all configurations of FishBAC stringers and corrugation unit cells, reducing the length of the unit cells decreases the mass of skin. The small jump in Fig. 10 is because the optimization algorithm has minimized the parameters t_c and t_e in a different way. As indicated in Table 4 the thickness of the core t_c attains the lower bound for the points with unit cell length less than 14.55 mm while for the points

Fig. 8 The trend of optimized objective function EA_{eq} for different lengths of unit cell

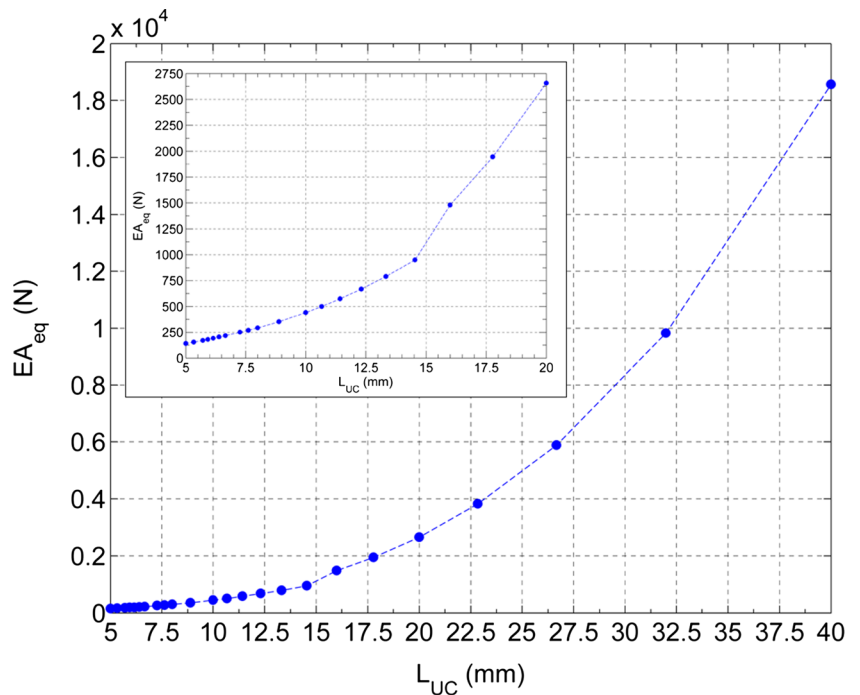
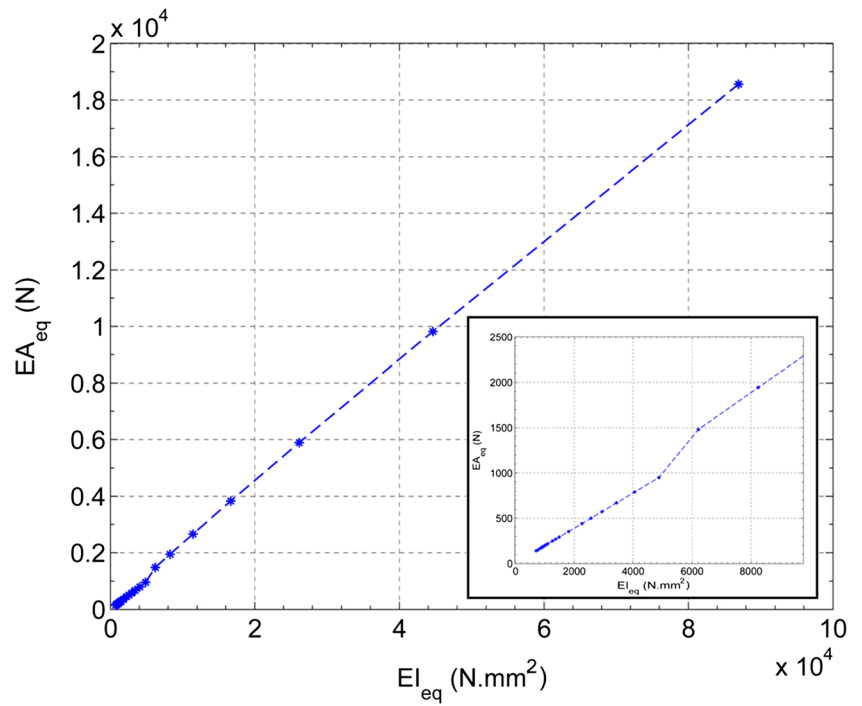


Fig. 9 The linear behaviour between the optimized in-plane stiffness and out of plane stiffness



with a unit cell length of more than 16 mm the thickness of the elastomer coating t_e has attained the lower bound.

Table 4 presents the optimized parameters and objectives of four points in the vicinity of the jump as highlighted in Fig. 10. The indices “lb” and “ub” represents the upper bound and lower bound of optimized parameters respectively. The optimization algorithm has also selected the corresponding values at the lower bound for the parameter a_2 , while for the

parameter h the upper bound is selected. This implies that increasing the height of the corrugation gives a higher ratio of bending stiffness to tensile stiffness.

Figure 11 shows the upper bounds, lower bounds and the trend of optimized parameter t_c and t_e for different lengths of unit cell. As illustrated in Fig. 11a the thickness of the corrugated core t_c , increases as the length of unit cells increases. As mentioned earlier, this ascending trend can be considered as

Fig. 10 The trend of optimized objective function “Mass” for different lengths of unit cell

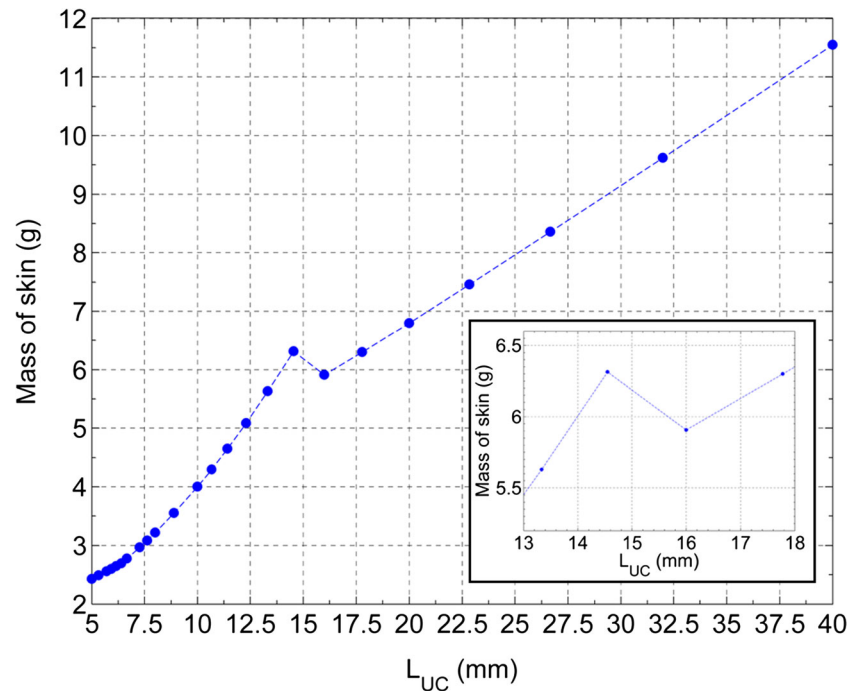


Table 4 The optimized parameters and objectives for four points in the vicinity of the jump highlighted in Fig. 10

L_{uc} (mm)	Real values of objectives			Optimized parameters					
	$\frac{1}{EI_{eq}}$ ($N \cdot mm^2$) ⁻¹	EA_{eq} (N)	Mass of skin (g)	t_c (mm)	t_e (mm)	a_1 (mm)	a_2 (mm)	a_3 (mm)	h (mm)
13.33	$2.47 \cdot 10^{-4}$	789.03	5.63	0.22 _{lb}	0.76	2.81	1.11 _{lb}	2.74	4.69 _{ub}
14.55	$2.05 \cdot 10^{-4}$	950.00	6.31	0.24 _{lb}	0.90	3.06	1.21 _{lb}	3.01	4.69 _{ub}
16	$1.61 \cdot 10^{-4}$	1479.42	5.91	0.46	0.27 _{lb}	3.33	1.33 _{lb}	3.33	4.69 _{ub}
17.78	$1.21 \cdot 10^{-4}$	1944.93	6.30	0.51	0.30 _{lb}	3.73	1.48 _{lb}	3.68	4.69 _{ub}

two phases. In the first phase, which is for unit cell lengths less than 14.55 mm, the parameter t_c has reached the lower bound in the optimization process. In the second phase, for unit cell lengths of more than 16 mm, the parameter t_c is optimized without approaching the bounds. The constant slopes in these two phases in Fig. 11a expresses that the ratio between the thickness of the core and the length of unit cell, $\frac{t_c}{L_{uc}}$ reaches a constant value in each phase. This constant value in the first phase is because of the optimization process which has selected the lower bound with a constant slope for the thickness of the corrugated core. However the value of $\frac{t_c}{L_{uc}}$ in the second phase, which is almost equal to 0.0275, is independent of the constant slopes of the bounds and implies that the optimized thickness of the core is linearly proportional to the length of unit cell. Moreover, Fig. 11b reveals that the thickness of the elastomer coating t_e , increases as the length of unit cells increases in both phases independently. In the first phase, for unit cell lengths less than 14.55 mm, the parameter t_e is optimized without approaching the bounds. In the second phase

which, for unit cell lengths more than 16 mm, the parameter t_e attains the lower bound in the optimization process and hence has a constant value of $\frac{t_e}{L_{uc}}$.

Figure 12 shows the upper bounds, lower bounds and the trend of parameters a_1 , a_2 and a_3 as a function of the length of the corrugation unit cell. The parameters a_1 and a_3 which represent the horizontal members of the corrugation geometry show a very close correlation as they are optimized. This means that there is a possibility of defining the geometry of corrugation with three parameters rather than four and it is likely to save more computation costs in future optimization studies. The ascending trend of parameters a_1 and a_3 can be considered in two phases. The first phase corresponding to the unit cell length smaller than 6.67 mm, is when the parameter a_2 has a descending trend, before reaching the lower bound. However in the second phase, which corresponds to a unit cell length of more than 6.67 mm, the parameter a_2 attains the lower bound which changes the descending trend into an ascending trend. The constant slope of the trends of the

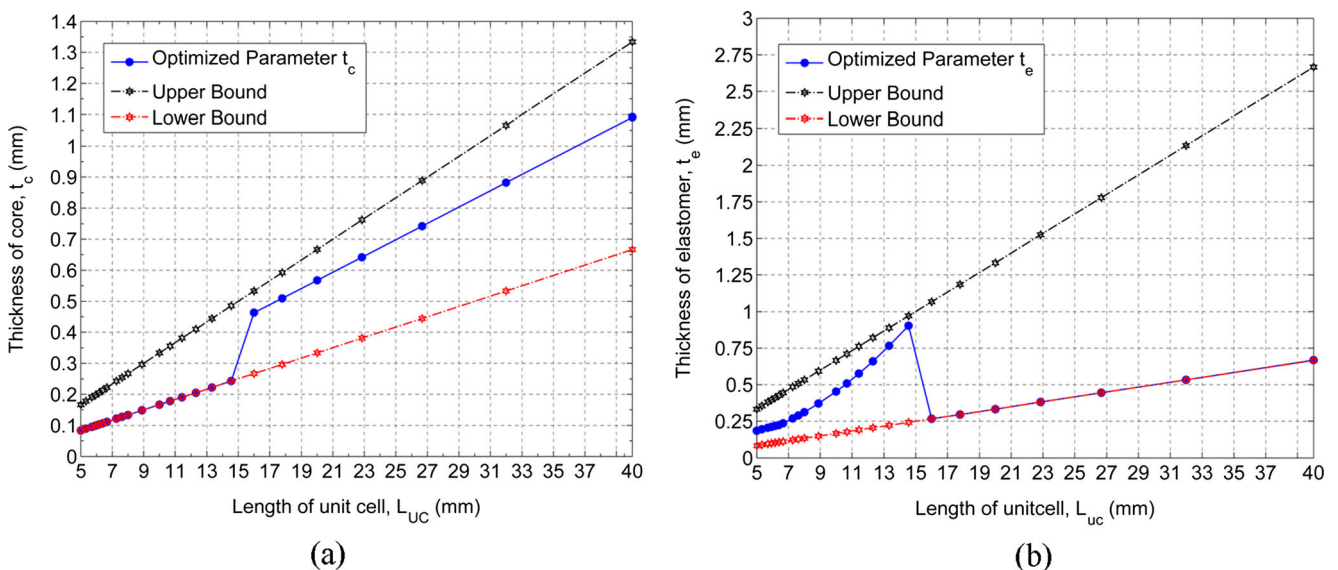
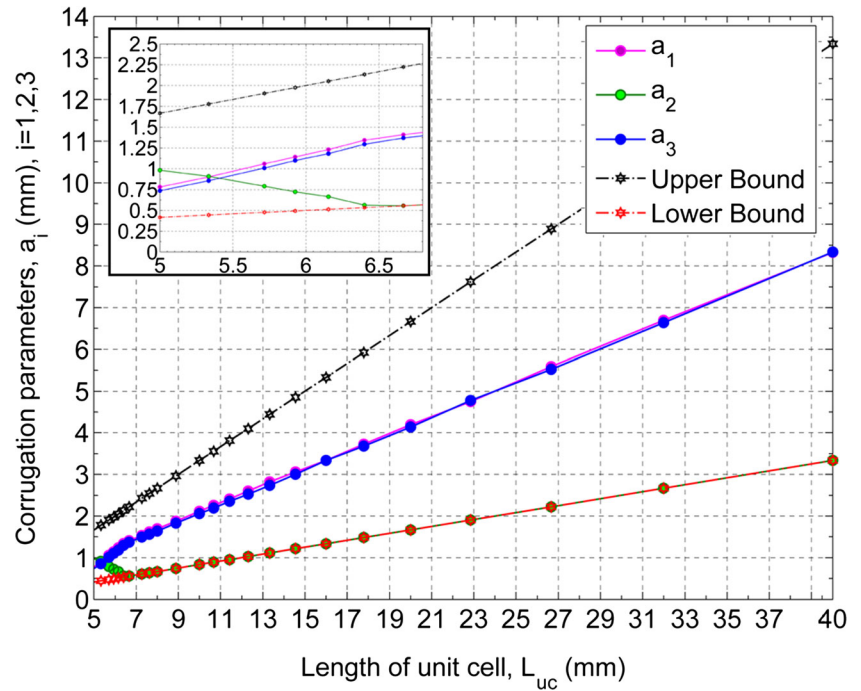


Fig. 11 Thickness of the corrugated core and the elastomeric coatings for different length of unit cells

Fig. 12 The upper bounds, lower bounds and the trend of parameters a_1 , a_2 and a_3 as a function of the length of corrugation unit cell

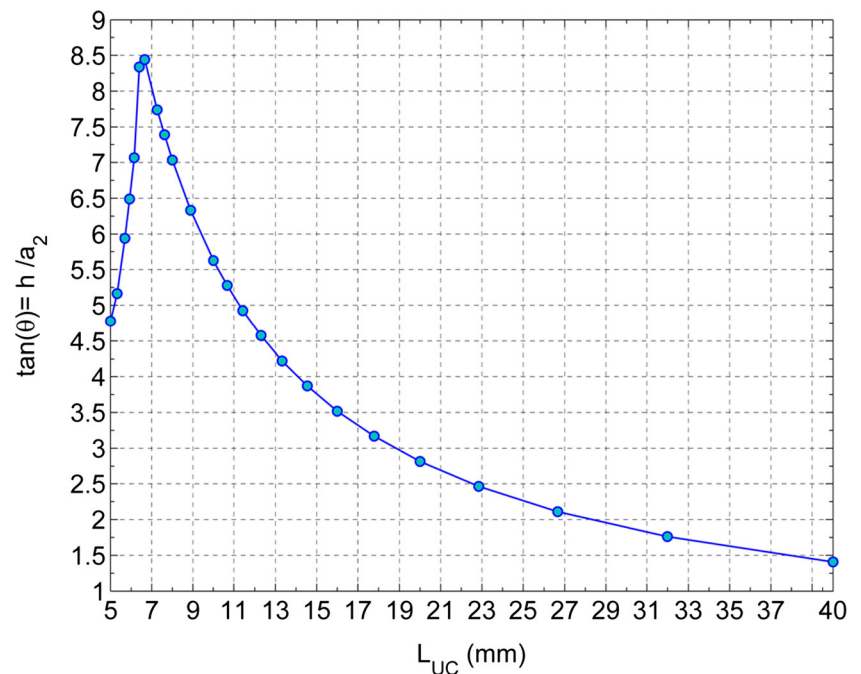


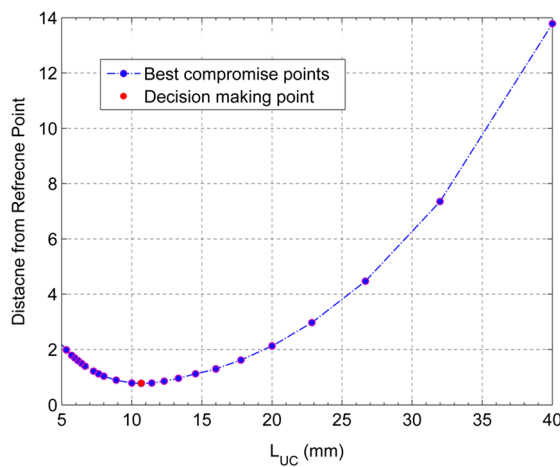
parameters a_1 and a_3 expresses the ratio of these parameters to the length of unit cells. The ratio of $\frac{a_1}{L_{uc}}$ and $\frac{a_3}{L_{uc}}$ in the first phase, where parameter a_2 has not reached the lower bound, is about 0.39. The slope of the trend of parameter a_2 is about -0.31 in the first phase which implies an inverse relationship between parameters a_2 and L_{uc} . However in the second phase, the constraint $a_1 + a_2 + a_3 = L_{hu}$ and the approximate equivalence $a_1 \approx a_3$ explains the constant slope of parameters a_1 and a_3 ,

which is because the parameter a_2 has hit the lower bound with a constant slope of 0.167.

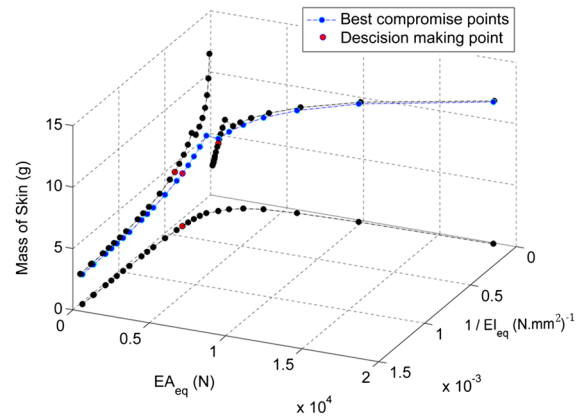
For the parameter h , which represents the height of the corrugation, the optimization algorithm has selected values at the upper bound. In many cases the optimization algorithm has selected the corresponding values at the lower bound for the parameter a_2 which implies that maximizing the angle of corrugation would result in a higher ratio of bending stiffness

Fig. 13 The optimized $\tan(\theta)$ as a function of the length of the unit cell





(a) Distance from ideal reference point



(b) Optimized objectives

Fig. 14 Entire best compromise points for different length of unit cells

to tensile stiffness. Figure 13 shows the optimized $\tan(\theta)$ as a function of the length of the unit cell.

In terms of design, the trend of the three optimized objectives at the best compromise points for the entire range of configurations of FishBAC stringers and corrugation unit cells are illustrated together in Fig. 14b. The design decision was made by repeating the process of finding the best compromise point among the optimized solutions in the normalized space of objectives. Figure 14a shows the distance of the best compromise points of different unit cell lengths to the ideal reference point presented in (2).

The decision point of the best design is highlighted as red in Fig. 14. However it must be mentioned that this point would be different if more importance is given to certain objective functions such as the in-plane compliance of the corrugated skin which reduces the required energy to morph. Table 5 shows the corresponding objective values and parameters at the decision point of the design. According to the Table 5 the length of a corrugation unit cell at the decision point is 10.67 mm. Consequently all of the configurations of FishBAC stringers and corrugation unit cells which are compatible in the equation of $(n_{stringer} + 1) \times N_{unitcell} = 15$ represent the highlighted decision point, i.e. cases 4.3, 5.2 and 14.1.

Table 5 Corresponding optimized parameters at the decision point of the design

Optimized objective functions			Optimized parameters (mm)					
$\frac{1}{EI_{eq}}$ (N.mm ²) ⁻¹	EA_{eq} (N)	Mass of skin (g)	t_c	t_e	a_1	a_2	a_3	h
3.9×10^{-4}	500.40	4.29	0.18	0.51	2.26	0.89	2.20	4.69

Although these cases have the same geometry of the skin, the number of the stringers of the FishBAC internal structure is different and hence the structural and aerodynamic characteristics of the assembled structure will be different. It is also possible to consider variable spacing of the stringers for the selected geometry of the skin. However such optimization and analysis are beyond the scope of this paper.

5 Conclusion

Morphing technology is necessary in the design of future aircraft as it provides the opportunity for the aircraft to adapt its shape in flight to the optimal configuration without unacceptable penalties in terms of cost, complexity and weight. Morphing technology increase the efficiency of aircraft in terms of fuel consumption, toxic emissions, noise pollution and maneuverability of the aircraft. However the requirements of morphing aircraft are conflicting from the structural perspective. For instance the design of a proper morphing skin is a huge challenge and a key issue since it must be stiff to withstand the aerodynamic loads, but flexible to enable the expected large shape changes. Corrugated sheets have remarkable anisotropic characteristics. As a candidate skin for a morphing wing, they are stiff to withstand the aerodynamic loads and flexible to enable the morphing deformations. In this paper the geometric parameters of the trapezoidal corrugated core with elastomeric coating are optimized to minimize the in-plane stiffness and the mass of the skin and to maximize the out-of-plane stiffness of the skin. To do so the equivalent tensile, flexural stiffness and the mass of a coated trapezoidal corrugated core were first calculated using a finite element code in MATLAB. Bearing in mind the

manufacturing limitations, different possible configurations of FishBAC stringers and corrugated skin were considered in the optimization problem. The upper bounds and the lower bounds of the geometric parameters of the corrugation were chosen carefully based on practical considerations, especially when the size of the corrugation was very small. The entire set of parameters of the corrugation were normalized in order to ensure the best performance of the optimization scheme. The advantages and limitations of the gradient based aggregate and the GA multi-objective method were investigated for solving the multi objective optimization problem for the corrugated skin. The results obtained from both methods were compared and finally the gradient based aggregate method was utilized in this paper. The dominance of each objective function due to the weight distribution in this method was discussed and highlighted on the Pareto surface of two sample cases. Moreover, by identifying the ideal reference point as the coordinates of minimum normalized objective values, the best compromise point was selected in each configuration of FishBAC stringers and corrugation unit cells. The range of the weights showed that all of the three objectives were involved efficiently in the process of optimization for the best compromise point. The trend of the optimized parameters and objectives were then investigated by collecting and studying the best compromise points in all the configurations of FishBAC stringers and corrugation unit cells. It was shown that the out of plane and in-plane compliances of the corrugated core with elastomeric coating decreased when the length of the corrugation unit cell increased. For almost all configurations of FishBAC stringers and corrugation unit cells, reducing the length of the unit cells decreased the mass of the skin. In terms of the trends of the optimized geometric parameters, it was shown that the thickness of the core attained the lower bound for the points with a unit cell length less than 14.55 mm, while for a unit cell length more than 16 mm the thickness of the elastomer coating reached the lower bound. This switch in the way that the optimization algorithm optimized these two parameters resulted in a small jump in the trend of objective function values. Moreover, the optimization algorithm selected the corresponding values at the lower bound for the parameter a_2 , while for the parameter h the upper bound was selected, implying that increasing the height of the corrugation gives a higher ratio of bending stiffness to tensile stiffness. Finally, the design decision was made by repeating the process of finding the best compromise point among the optimized solutions in a normalized space of objectives. The length of a corrugation unit cell at the decision point was 10.67 mm and hence several

configurations of FishBAC stringers and corrugation unit cells were compatible with the highlighted decision point, i.e. cases 4.3, 5.2 and 14.1.

Acknowledgments The authors acknowledge funding from the European Research Council through Grant No. 247045 entitled “Optimisation of Multiscale Structures with Applications to Morphing Aircraft”.

Open Access This article is distributed under the terms of the Creative Commons Attribution 4.0 International License (<http://creativecommons.org/licenses/by/4.0/>), which permits unrestricted use, distribution, and reproduction in any medium, provided you give appropriate credit to the original author(s) and the source, provide a link to the Creative Commons license, and indicate if changes were made.

References

- Barbarino S, Bilgen O, Ajaj RM, Friswell MI et al (2011) A review of morphing aircraft. *J Intell Mater Syst Struct* 22(9):823–877
- Bartolozzi G, Baldanzini N, Pierini M (2014) Equivalent properties for corrugated cores of sandwich structures: a general analytical method. *Compos Struct* 108:736–746
- Chekkal I, Cheung R, Wales C, Cooper JE et al (2014) Design of a morphing wing tip. AIAA Scitech Conference, National Harbor, pp 13–17
- Das I, Dennis JE (1997) A closer look at drawbacks of minimizing weighted sums of objectives for Pareto set generation in multicriteria optimization problems. *Struct Optim* 14(1):63–69
- Dayyani I, Ziaei-Rad S, Friswell MI (2013) The mechanical behavior of composite corrugated core coated with elastomer for morphing skins. *J Compos Mater* 104:281–292
- Dayyani I, Friswell MI, Flores EIS (2014) A general super element for a curved beam. *Int J Solids Struct* 51(17):2931–2939
- Dayyani I, Shaw AD, Saavedra Flores EI, Friswell MI (2015a) The mechanics of composite corrugated structures: a review with applications in morphing aircraft. *Compos Struct* 133: 358–380
- Dayyani I, Haddad Khodaparast H, Woods BKS, Friswell MI (2015b) The design of a coated composite corrugated skin for the camber morphing airfoil. *J Intell Mater Syst Struct* 26(13):1592–1608
- Deb K (2001) Multi-objective optimization using evolutionary algorithms, vol. 16. Wiley
- Gilchrist AC, Suhling JC, Urbanik TJ (1999) Nonlinear finite element modeling of corrugated board. *Mech Cellul Mater SME, AMD-Vol. 231/MD-Vol. 85*
- Goldberg DE, Holland JH (1988) Genetic algorithms and machine learning. *Mach Learn* 3(2):95–99
- Hochman HM, Rodgers JD (1969) Pareto optimal redistribution. *Am Econ Rev* 542–557
- Izui K et al (2015) Multiobjective optimization using an aggregative gradient-based method. *Struct Multidiscip Optim* 51.1:173–182
- Li X, Wang Z, Zhu F, Wu G, Zhao L (2014) Response of aluminium corrugated sandwich panels under air blast loadings: experiment and numerical simulation. *Int J Impact Eng* 65:79–88
- Luo S, Suhling JC, Considine JM, Laufenberg TL (1992) The bending stiffness of corrugated board. *Mech Cellul Mater ASME, AMD-Vol. 145/MD-Vol. 36*
- Marler RT, Arora JS (2004) Survey of multi-objective optimization methods for engineering. *Struct Multidiscip Optim* 26(6):369–395

- Mohammadi H, Ziaei-Rad S, Dayyani I (2015) An equivalent model for trapezoidal corrugated cores based on homogenization method. *Compos Struct* 131:160–170
- Munk DJ, Vio GA, Steven GP (2015) Topology and shape optimization methods using evolutionary algorithms: a review. *Struct Multidiscip Optim* 52(3):613–631
- Peng M, Liu P, Cheng Y (2014) Free vibration analysis of corrugated-core sandwich plates using a mesh free Galerkin method based on the first-order shear deformation theory. *Int J Mech Sci* 78:8–18
- Shaw AD, Dayyani I, Friswell MI (2015) Optimisation of composite corrugated skins for buckling in morphing aircraft. *Compos Struct* 119:227–237
- Zhang WH, Gao T (2006) A min–max method with adaptive weightings for uniformly spaced Pareto optimum points. *Comput Struct* 84(28):1760–1769
- Zhang L, Hebert R, Wright JT, Shukla A, Kim JH (2014) Dynamic response of corrugated sandwich steel plates with graded cores. *Int J Impact Eng* 65:185–194